01 Jan 1982

D- Production By Charge Transfer Of (0.3 - 3)-keV D+ In Thick Alkaline-earth Vapor Targets: Interaction Energies For CaH+, CaH, And CaH-

R. (Robert) H. McFarland
Missouri University of Science and Technology

A. S. Schlachter

J. W. Stearns

B. Liu

et. al. For a complete list of authors, see https://scholarsmine.mst.edu/phys_facwork/2565

Recommended Citation

R. H. McFarland et al., "D- Production By Charge Transfer Of (0.3 - 3)-keV D+ In Thick Alkaline-earth Vapor Targets: Interaction Energies For CaH+, CaH, And CaH-," *Physical Review A*, vol. 26, no. 2, pp. 775 - 785, American Physical Society, Jan 1982.
The definitive version is available at https://doi.org/10.1103/PhysRevA.26.775

D^- production by charge transfer of (0.3—3)-keV D^+ in thick alkaline-earth vapor targets: Interaction energies for CaH^+, CaH, and CaH^-

R. H. McFarland,* A. S. Schlachter, J. W. Stearns, B. Liu,† and R. E. Olson*
Lawrence Berkeley Laboratory, University of California, Berkeley, California 94720
(Received 7 December 1981)

Equilibrium charge-state fractions of energetic deuterium ions and atoms emerging from alkaline-earth (magnesium, calcium, strontium, and barium) vapor targets are reported in the range of 0.3- to 3-keV incident D^+ energy. Deuterium negative-ion production in thick barium and calcium vapor targets equals similar production in cesium vapor ($\sim 34\%$). Moreover, the maxium D^- production in strontium vapor exceeds that for all other known gas or vapor targets and reaches 50% at 500 eV. Theory does not quantitatively describe these results, although *ab initio* molecular-interaction-energy calculations on the neutral and negative-ion CaH systems lead to the prediction of large D^- yields at low energies. The theoretical prediction is based on the lack of a strong coupling between the negative-ion and neutral molecular states. This implies that there are small D^- electron-detachment cross sections at energies less than 1 keV. The present measurements agree with previous measurements done at higher energies.

I. INTRODUCTION

In a recent paper, Schlachter *et al.*[1] discussed in some detail the earlier literature and the importance of D^- production in the fueling and heating of fusion plasmas. They also presented the equilibrium charge-state fractions F_-^∞, F_0^∞, and F_+^∞ for D^+ and D^- incident on cesium, rubidium, and sodium vapor in the energy range of 0.3 to 10 keV. Although there have been a number of investigations in which alkali-metal vapor targets have been used, little work has been performed on alkaline-earth vapor targets at energies less than 2 keV. Earlier investigators[2,3] presented data for magnesium and strontium vapor targets at higher energies and compared the measured F_-^∞ fractions with those of the alkalis. Their measurements of D^- yields in strontium vapor started to rise unexpectedly at lower energies. Recent experimental observations by Morgan *et al.*[4] and theoretical calculations by Olson[5] indicate that the alkaline-earth vapor targets may have high negative-ion yields at low energies. The purpose of this paper is to present data for these systems.

The production of D^- is predominantly one that involves successive charge-changing collisions. The collisional cross sections which dominate at these energies are σ_{+0}, σ_{0-}, and σ_{-0}, which, respectively, involve the interactions with a target X as follows:

$$D^+ + X \rightarrow D^0 + X^+ \quad (\sigma_{+0}) , \tag{1}$$

$$D^0 + X \rightarrow D^- + X^+ \quad (\sigma_{0-}) , \tag{2}$$

and

$$D^- + X \rightarrow D^0 + \begin{Bmatrix} X + e^- \\ X^- \end{Bmatrix} \quad (\sigma_{-0}) . \tag{3}$$

The three remaining cross sections (σ_{+-}, σ_{0+}, σ_{-+}) contribute significantly only to F_+^∞ which is observed to be very small at low energies. The electronic levels populated after the electron-capture reaction (1) have not been identified. However, measurements of the population of the high-n states[6] and molecular structure calculations[5] support the assumption that a large fraction of the atoms are initially produced in the ground state.

The equilibrium fraction of the beam exiting the target in charge state i, represented by F_i, is

$$F_i^\infty = \lim_{\pi \rightarrow \infty} F_i(\pi) , \tag{4}$$

where, for target line density π, $F_i(\pi)$ represents the equivalent density-dependent fraction.

For the range of targets and energies studies here, the D^- fraction becomes constant as π approaches 10^{16} cm^{-2}, while the D^+ fraction has become negligibly small. Under these conditions, F_0^∞ and F_-^∞ are represented by the D^0 and D^- fractions and are determined by the competing processes (2) and (3). It is easily shown that

$$F_-^\infty = \frac{\sigma_{0-}}{\sigma_{0-} + \sigma_{-0}} \tag{5}$$

and

$$F_0^\infty = \frac{\sigma_{-0}}{\sigma_{0-} + \sigma_{-0}} , \tag{6}$$

thus

$$\frac{\sigma_{-0}}{\sigma_{0-}} = \frac{F_0^\infty}{F_-^\infty} . \tag{7}$$

In this paper, measurements are presented for F_i^∞ versus energy resulting from D^+ interacting with alkaline-earth vapor targets. In order to understand the experimental results, the interaction energies for the ground states of the calcium hydride ionic and neutral systems have been calculated. These calculations should serve as exemplary prototypes for the heavier alkaline-earth-hydride systems, because the ionization potential of calcium is reasonably close to that of strontium and barium. The goal of the calculations is to answer questions as to whether or not the negative molecular ion is bound and stable to electron detachment and whether the negative and neutral molecular states are well separated in energy at intermediate to large internuclear separations.

II. EXPERIMENTAL METHOD

A. General description

Improvements in neutral-particle detection systems have made it possible to extend F_i measurements to energies as low as 300 eV. A D^+ beam, after traversing a metal-vapor target and undergoing charge-changing reactions, was analyzed by a short transverse electric field into its D^+, D^0, and D^- components. The D^+ and D^- components were collected in Faraday cups, and a pyroelectric ceramic disk was used to measure the D^0. A schematic diagram of the apparatus is shown in Fig. 1.

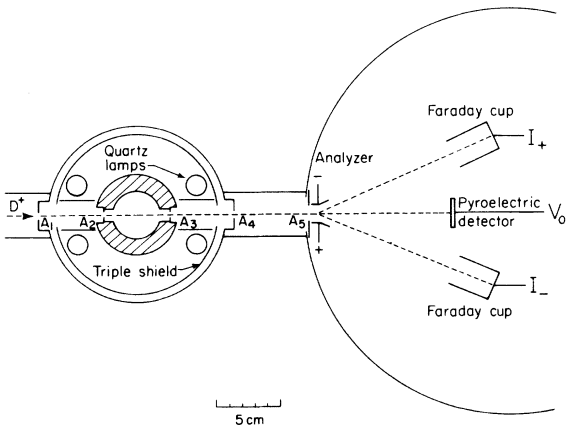

FIG. 1. Schematic diagram of the target and analyzer chambers. Aperture sizes A_1 and A_4, 0.381 cm; A_2 and A_3, 0.287 cm; and A_5, 1.02 cm. The horizontal scale is indicated.

B. Ion beam

The positive deuterium ions were extracted from a duoplasmatron at full acceleration potential, focused by an Einzel Lens, steered, and electrostatically chopped with a 50% duty cycle at 3 Hz. A magnetic field was used to select the D^+ from the molecular ions and from the fast neutrals produced by collision in the background gases. A precision voltage divider was used to regulate and determine the accelerating potential difference to an uncertainty of less than 0.1%. This potential difference approximated closely the potential through which the ions fell and determined their energy to about 10 eV. Modulated currents observed at the detectors with the oven at room temperature ranged from 3 to 30 nA.

C. Target

Because of the higher temperatures required to provide suitable target densities for alkaline-earth vapors, it was necessary to modify an older target oven[7] that had been designed to contain a lithium vapor target. Heat pipes suitable for cesium could not be used, because the alkaline earths sublime (rather than melt) at the temperature required to produce the needed vapor pressure. A heavy, mild steel container, with Chromel-Alumel thermocouples buried in its walls at the top and bottom of the oven, was employed. Heat was provided by four 750-W quartz lamps as shown in Fig. 1. These lamps were operated in a series-parallel configuration from a temperature-regulated controller which used one of the embedded thermocouples for feedback. During the equilibrium measurements, the controller was normally bypassed. Heating was regulated by the operator, who employed a series inductance to provide the slowly increasing or decreasing temperatures required. Temperatures as high as 1200 K were used during one outgassing sequence without lamp failure. An occasional rupture of the quartz-lamp envelope was traceable to a chemical reaction of the target vapors with quartz. Infrequent shorting of the lamp leads occurred when metal deposits from nearby grounded locations peeled off and came in contact with unprotected portions of the lead wires. Otherwise, this method of heating the target chamber was entirely satisfactory.

The length of the oven was 4.6 cm. The temperatures were read from the thermocouples, and vapor pressure tables[8] were used to convert them into appropriate number densities. The resulting line den-

sity should be regarded as a lower limit. We estimate the effective target length to vary in the range 10 ± 5 cm, because the method of heating produced target vapor at an unknown density external to the oven. As the measurement of $F^{\infty}_{=}$ was our primary interest, line density as an absolute was of secondary importance. Oven number densities of 5×10^{14} atoms/cm^3 were usually sufficient to achieve a constant D^- fraction, which corresponds to line densities of roughly (2 to 5)$\times10^{15}$ atoms/cm^2. For a few high-energy measurements, number densities as high as 2×10^{15} atoms/cm^3 were reached to confirm equilibrium.

D. Detection and data acquisition

At equilibrium, each atom emerging from the oven experiences sufficient charge-changing collisions so that the charge-state ratios are expected to be the same for all emergent angles.[1] Thus, one may limit the size of the emergent beam and still retain the proportionality of each charge state. The need for limitation was determined by the size of the active surface of the neutral detector, whose diameter was approximately 2.3 cm. The magnetically suppressed Faraday cups were of larger diameters. Apertures A_3, A_4, and A_5, 0.287, 0.381, and 1.02 cm, respectively, shown in Fig. 1, provided this geometric limiting function. [A_1 (0.381 cm), A_2 (0.287 cm), A_3, and A_4 served to limit loss of target material from the oven and chamber.] The beam was electrostatically analyzed with a voltage selected so as to center the charged beams on the Faraday cups.

The analyzer voltage range, observed when the oven was hot, for which the Faraday-cup currents remained constant, was more than two-thirds the centering voltage, which confirmed the limited size of the beam.

The neutral detector warrants discussion, because it reliably measured neutral equivalent currents in the 10^{-11}-A range for particles of 300-eV energy. It could have been operated at lower power levels had there been a need. The detector was a pyroelectric, lead-zirconate-titanate, ceramic disk (Gulton G1500) with a thin silver coating on each face. The theory of such a detector has been discussed[9,10] as has its general mode of operation. The bombarding particles heat the detector which produces a change in the potential difference between the two faces. A modulated beam, charged or neutral, falling on one of the faces produces a modulated voltage, which can be phase detected and analyzed as directly proportional to the power input to the detector, thus allowing calibration with charged particles. Division by the beam energy provides an equivalent flux calibration.

A phase-sensitive detector (Ithaco Dynatrac 3) was used to preamplify and measure the detector voltage signal. The two Faraday-cup currents were measured with Keithley 610C electrometers. The voltage outputs of all three circuits were employed to drive three locally made integrators. A master control unit provided either constant-time or constant-charge simultaneous integrations for the three detectors which were all calibrated relative to each other. A specific advantage of these integrators is that they allow for both positive and negative integrations. This was necessary at times for low neutral-detector power levels when random-phase electrical noise could be momentarily larger than the signal.

Although the neutral detector has an output voltage signal versus neutral particle flux ratio K, which remains constant throughout its use, its measured value may not, depending on conditions of circuity and cleanliness. Pyroelectric material is also microphonic; for this reason the detector holder must have a built-in shock mounting. The electrical contacts to the detector must be as resistance free as possible because, during the calibration process, currents incident on the front face that are not fully shorted to ground will mix with the signal and change both its magnitude and phase relative to the beam. This problem is alleviated as the ratio of the incident power to charged current is increased and is not associated with neutral power measurements. A shift of phase or a change in the measured K calibration ratio is an indication of the possibility of poor contacts or improper front-face grounding. This effect has been appreciably reduced by mounting the detector rigidly between the two electrical contacting surfaces and providing a shock-absorbing mounting between the holder and the vacuum chamber.

Power reflection was also a potential source of error in these measurements; however, the linear response of the detector over several orders of magnitude of beam energy and power input, as shown in Fig. 2, indicates that this effect is negligible. Biasing experiments have also been performed, in which the detector has been biased both positively and negatively with respect to ground; the deflection plates in front of the detector were biased with respect to the dectector, and the charged beam was deflected by small incremental voltages to move to alternate locations across the detector. These experiments failed to produce any variation in experi-

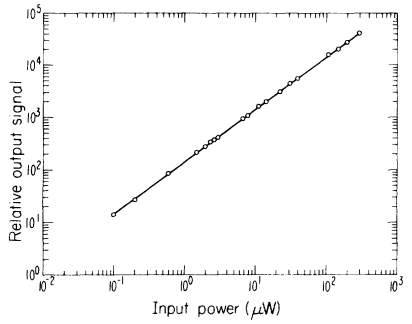

FIG. 2. Plot of the neutral-detector output as a function of input power. Typically these pyroelectric ceramic disks develop about a microvolt response for a microwatt input with the circuitry following the detector determining the magnitude of the relative signal observed.

mental results that would indicate an error in neutral-beam detection.

There was a small secondary dependence in K on temperature change, that was removed when the power input was kept constant. This effect is less than 5% over the entire power range observed. Constant-temperature effects, such as those caused by radiant heat from the oven or from the beam power, were small and were nullified when the value of K was measured under the same experimental conditions as the F_i fractions.

Frequent cleaning was required because the target metals deposited on the aperatures and the neutral detector deteriorated upon prolonged exposure to the vacuum background gases and produced chargeable surfaces. To assure constant neutral detection efficiency, K was measured prior to and after almost every set of F_i measurements. Data were discarded for runs in which K changed more than 5%. Electrical ground loops, another source of signal noise and error, were avoided. Lead wires were kept as short, flexible, low loss, and well shielded as possible. Obviously, the back face of the detector and its lead were especially vulnerable to stray electrons and were protected. Although neutral currents involving power levels of the order of a few nW were reliably measured during the course of the experiments, K values were normally measured at power levels of 100 nW or more. K measurements required stable conditions, because the signals for two different but equal-length time periods were being compared, whereas F_i measurements involved signals during the same time period.

A Hewlett-Packard 9845B desk-top computer read the three integrators, the energy of the beam, the temperature of the oven, the integrating time, and the Hall-probe voltage monitoring the bending magnet. It further performed the functions of analyzing the data and plotting them. Thus, plots of the three current fractions and total current versus number density were available for each target species and energy measured. Examples are given in Figs. 3 and 4, which show the variation of the charge-state fractions with number and estimated line density, including the equilibrium plateaus. The total emergent particle current decreases logarithmically with target density by amounts ranging from 50 to 90%, depending on the geometry and energy. Although the measurements extend far into the thick-target regime, near equilibrium fractions may be identified at line densities of about 5×10^{15} cm^{-2}, at which the total beam current is still a significant fraction of the initial beam. Optimization of D^- production near this line density would be practical in the development of a negative-ion source.

E. Procedure

The oven and analyzing chambers had to be cleaned chemically before loading or reloading target material. The oven was then loaded with 99.9% pure target metal, evacuated, and slowly heated to above the expected equilibrium temperature. It was then allowed to cool to temperatures below the on-

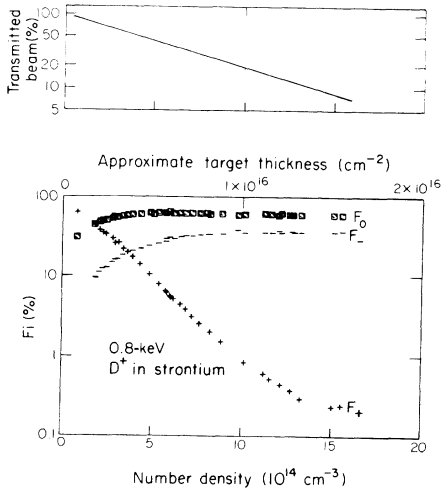

FIG. 3. Charge component yields F_i and transmitted beam percentage vs number and line densities for 800-eV D^+ in strontium vapor. Line density has an estimated error of 50% for reasons given in the text. The fractions shown for target thicknesses less than equilibrium are not accurate because of likely unequal loss of the beam components.

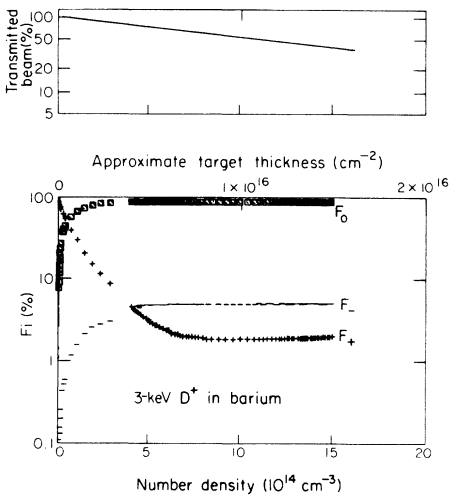

FIG. 4. Charge component yields F_i and transmitted beam percentage vs number and line densities for 3-keV D^+ in barium vapor. Remarks are the same as for Fig. 3.

set of charge-state equilibrium K (the pyroelectric detector calibration) was measured, and measurements of the charged- and neutral-beam fractions were then made with the temperature slowly increasing until equilibrium density was exceeded. Successive measurements of about 100-s duration were continued through the heating and cooling cycles. From the computer plot of F_i versus density (see, e.g., Fig. 3), a number density was chosen where F_i appeared to have reached its equilibrium value, and all measurements (as many as 150) above that density were averaged to determine each equilibrium fraction. The decreasing temperature measurements of F_{-}^{∞} tended to be higher than those with an increasing temperature, which seemed to be due to the background pressure of the order of 10^{-6} Torr being lower during the cooling phase. We estimate that any error due to this effect that was not corrected for would cause us to underestimate F_{-}^{∞} by at most 2% (one percentage point at a yield of 50%).

III. METHOD OF CALCULATION

Approximations to the Born-Oppenheimer electronic wave functions and energies were calculated by using self-consistent-field (SCF) and configuration-interaction (CI) methods. An electronic wave function was expanded in an orthonormal, n-particle basis set of $C_{\infty v}$ symmetry-and-equivalence–restricted configuration-state functions (CSF). These CSF's were linear combinations of Slater determinants, such that each had the symmetry and multiplicity of the molecular state under consideration. The Slater determinants were constructed from an orthonormal set of basis orbitals, which were expanded in terms of an elementary basis set of Slater-type functions centered at the atomic nuclei. The calculations were performed by using ALCHEMY, a system of programs for the calculations of molecular wave functions developed at IBM by Bagus, Liu, McLean, and Yoshimine.

The Slater-type-function basis sets employed in the calculations are given in Table I. The H basis set is from the work of Liu *et al.*[11] with the 4*d* and 4*f* functions deleted because they were deemed unnecessary for the calculations. This basis set primarily originated from the complete CI wave function of H^- obtained by Weiss.[12] The H basis set presented in Table I yields the exact energy for H to six decimal places and a dipole polarizability of $4.4993a_0^2$ ($1a_0=0.5291F\times10^{-8}$ cm). The CI energy computed for H^- is $-0.527\,159$ a.u., which translates to an electron affinity of 0.739 eV. The measured electron affinity for H is 0.754 eV.[13]

The calcium basis set originated with the (11*s*/6*p*) basis given by Clementi and Roetti.[14] This basis was augmented with two 4*p* functions and three 3*d* functions. The optimization procedure for these five functions has been described by Liu and Olson.[15] To determine the quality of the calcium

TABLE I. Slater-orbital basis sets.

H	1*s*	1.60	Ca	1*s*	32.150 0
		1.10			19.973 1
		0.45		2*s*	17.239 4
	2*s*	1.10			8.403 61
		0.45		3*s*	7.469 07
	2*p*	1.20			3.959 36
		0.85			3.016 57
	3*d*	1.70		4*s*	3.091 05
					1.628 84
					1.012 03
					0.667 33
				2*p*	15.994 7
					9.129 15
				3*p*	7.377 79
					3.629 74
					2.348 62
					1.640 38
				4*p*	1.094 2
					0.697 7
				3*d*	4.766 66
					2.122 2
					0.800 7

basis, two sets of CI calculations were performed to compute the atomic parameters. In the first calculation, termed V for valence, the K, L, and M shells of calcium were kept fully occupied, and all single- and double-electron excitations out of the $4s\sigma^2$ level were allowed. In the second calculation, termed CV for core valence, the K and L shells were kept fully occupied, and all single and double exictations from the M and the $4s^2$ valence shells were allowed with the restriction that only single excitations from the M shell be allowed. Thus, the V calculation included only the electronic correlation energy of the valence shell, whereas the CV calculation also included the correlation energy between the M and valence shells. The number of configurations of the V and CV calculations were 204 and 2272, respectively. A complementary set of calculations were also performed on Ca^+ in order to determine the ionization potentials. Here, the number of configurations was 17 and 1135 for the V and CV calculations, respectively.

The results of a Hartree-Fock (HF) and the V and CV CI calculations for the ionization potential of calcium were 5.12, 5.90, and 6.04 eV, respectively. The spectroscopic value is 6.11 eV.[16] For the dipole polarizability, one obtains 185.2, 178.9, and $158.5a_0^3$, respectively, for the same set of calculations. The experimental value for the dipole polarizability[17] is $169\pm17a_0^3$, whereas the accurate CI calculations of Reinsch and Meyer[18] place the value at $153.9a_0^3$. Thus, for high accuracy, a CV type of CI calculation must be employed. At this time, only a CV calculation on the $X\,^1\Sigma$ state of CaH^+ was performed. The other molecular calculations are reported at the V level.

In the molecular calculations for CaH, an SCF calculation was first performed on the $X\,^2\Sigma$ state of CaH to determine the spatial orbitals. The CI calculation, which is termed valence V, was then made in which the 1σ to 5σ and 1π and 2π orbitals were kept fully occupied. The remaining orbitals were divided into two sets: the 6σ and 7σ valence orbitals which correlate with calcium $4s$ and H $1s$, and the virtual orbitals. The CSF's for the CaH V calculations were generated by allowing all single and double excitations from the valence to the virtual orbitals with respect to the above configuration. The number of configurations for the calculation was 1472.

In the molecular calculations for CaH^-, and SCF calculation was first performed on the $X\,^1\Sigma$ state of CaH^- to determine the spatial orbitals. A V-type CI calculation was then executed. This was completely analogous to the CaH calculation. The number of configurations was 1464.

For the CaH^+ systems, an SCF calculation was first performed on the $^2\Sigma$ state of $Ca^+ + H^+$ to determine the spatial orbitals. For the $X\,^1\Sigma$ state, two sets of CI calculations, V and CV, were then performed. In all the calculations, the 1σ to 3σ and the 1π orbitals were kept fully occupied. The remaining orbitals were divided into three sets: the calcium $3s$ and $3p$ inner shell consisting of the 4σ, 5σ, and 2π orbitals; the 6σ to 8σ valence orbitals, which correlate with H $1s$ and calcium $4s$ and $4p$; and the virtual orbitals. The CSF's and the CaH^+ V calculations were generated by allowing all single and double excitations from the valence orbitals to the virtual orbitals with respect to the reference configuration. The number of configurations for the $X\,^1\Sigma$ and $a\,^3\Sigma$ calculation were 413 and 372, respectively. The CSF's for the CV calculations on the $X\,^1\Sigma$ state included single and double excitations from both the inner and valence sets except for the restriction that only single excitations from the inner shell were allowed. Again, these excitations were with respect to the reference states given above. Thus, the V calculations included the electronic correlation energy of the valence shell, whereas the CV calculations also included the correlation energy between the valence and inner shells. The number of configurations for the CV calculation on the $X\,^1\Sigma$ state of CaH^+ was 6669.

IV. EXPERIMENTAL RESULTS AND UNCERTAINTIES

The results of these measurements are shown graphically in Figs. 5 through 8 and are listed in Table II. The uncertainties shown in Table II are the standard deviations of the means representing many measurements (up to 150) taken over integration times of from 20 to 300 s combined in quadratures with the equivalent uncertainties associated with the calibration of the neutral detector. All the measurements were repeated; repetitive measurements with minor changes in the geometry, different neutral detectors and chopping frequencies, and target metals from different lots, fall within less than 5% of each other and within one percentage point at high energies. Agreement with previous results,[2–4] where they overlap with present results, is excellent for magnesium, calcium, and strontium vapor targets. For barium, the low-energy data are consistently higher than those of Morgan *et al.*[4] (but within the combined standard error), who suggested that their data were as much as 10% low because the temperature of their oven

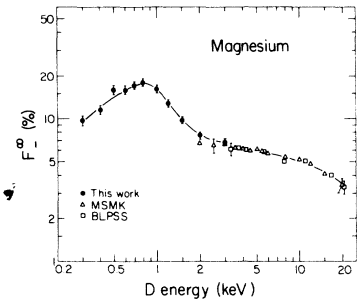

FIG. 5. Equilibrium yield F_-^∞ for D in magnesium vapor. Symbols: ●, present results; △ (MSMK), Morgan *et al.* (Ref. 4); □ (BLPSS), Berkner *et al.* (Ref. 2). The line is drawn for clarity.

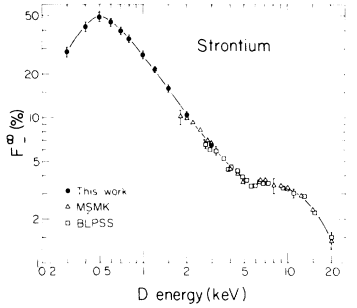

FIG. 7. Equilibrium yield F_-^∞ for D in strontium vapor. Symbols: ●, present result; △ (MSMK), Morgan *et al.* (Ref. 4); □ (BLPSS), Berkner *et al.* (Ref. 3). The line is drawn for clarity.

may not have been sufficient to achieve charge-state-fraction equilibrium. Figure 9 shows a composite of $F_\pm^\infty$ fractions produced in metal vapors. This composite includes measurements made by authors cited earlier.

Many of the F_+^∞ results are tabulated as upper limits because, except for the higher-energy measurements, they fail to reach equilibrium values even for much thicker targets than the F_- and F_0 fractions. Thus, an entry <0.1 means that, although the fraction had been observed to be as low as 0.1%, the D^+ fraction was still decreasing exponentially at the thickest target used. The experiment was terminated at that point to avoid unnecessary loss of the target material and resulting contamination of the collimators and detector.

The σ_{-0}/σ_{0-} ratios tabulated suggest the desirability of further cross-section measurements, because knowledge of either provides knowledge of the other, due to the relatively small values obtained for F_+^∞.

Although the repetition variances and statistical errors are small, possible uncertainties still remain with respect to the neutral detector, the charged-particle detectors, and the statistics of the measurements. Of these, only the neutral detector and the statistics of measurement contribute substantially to the standard error. The electrometers used to measure charged-particle current are absolute only to $\pm 3\%$; however, since F_i^∞ is a ratio, absolute current is not required, and error introduced by the detector circuitry is less than 1%. The statistical standard error in measuring K was usually about 3%. Similarly, with the large number of observations involving adequate integrating times, the standard error of the plateau measurements was normally less than 1%. Thus, the experimental standard error should not exceed 5%, and is much less at higher energies. This is consistent with repetitive measurements made in the present research and duplication of results at higher energies of the work of others.

V. COMPUTATIONAL RESULTS

The results of the V calculations on the CaH ionic and neutral systems are given in Tables III and IV and presented graphically in Fig. 10. A compi-

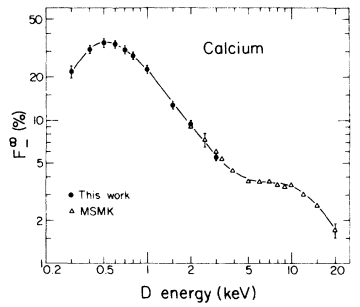

FIG. 6. Equilibrium yield F_-^∞ for D in calcium vapor. Symbols: ●, present results; △ (MSMK) Morgan *et al.* (Ref. 4). The line is drawn for clarity.

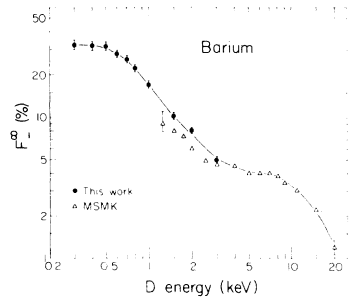

FIG. 8. Equilibrium yield F_-^∞ for D in barium vapor. Symbols: ●, present result; △ (MSMK), Morgan *et al.* (Ref. 4). The line is drawn for clarity.

TABLE II. Equilibrium fractions including standard errors and cross-section ratios.

Energy (eV)	Magnesium F^{∞}_{-} (%)	F^{∞}_{0} (%)	F^{∞}_{+} (%)	$\frac{\sigma_{-0}}{\sigma_{0-}}$	Calcium F^{∞}_{-} (%)	F^{∞}_{0} (%)	F^{∞}_{+} (%)	$\frac{\sigma_{-0}}{\sigma_{0-}}$
300	9.7±0.6	90.2∓0.6	<0.1	9.3	21.8±2.2	78.0∓2.2	<0.2	3.6
400	11.5±0.5	88.4∓0.5	<0.1	7.7	31.3±1.2	68.5∓1.2	<0.2	2.2
500	15.7±0.7	84.2∓0.7	<0.1	5.4	34.3±1.2	65.5∓1.2	<0.2	1.9
600	15.8±0.7	84.1∓0.7	<0.1	5.3	33.9±1.4	65.9∓1.4	<0.2	1.9
700	17.1±0.8	82.8∓0.8	<0.1	4.9	30.9±1.1	68.9∓1.1	<0.2	2.2
800	17.9±0.8	82.0∓0.8	<0.1	4.6	28.0±1.0	71.7∓1.0	<0.3	2.6
1000	16.1±0.7	83.8∓0.7	<0.1	5.2	22.5±1.1	77.1∓1.1	<0.4	3.4
1200	12.8±0.6	87.0∓0.6	<0.2	6.8				
1500	9.7±0.5	90.0∓0.5	0.3±0.1	9.2	12.7±1.1	86.0∓1.1	1.3±0.3	6.8
2000	7.6±0.5	92.1∓0.5	0.3±0.1	12.1	9.4±0.5	88.3∓0.5	2.3±0.1	
3000	6.8±0.4	92.2∓0.4	1.0±0.1		5.5±0.2	90.3∓0.2	4.2±0.1	
		Strontium				Barium		
300	29.1±1.2	70.7∓1.2	<0.2	2.4	33.0±1.3	66.9∓1.3	<0.1	2.0
400	44.0±1.3	55.8∓1.3	<0.2	1.3	32.4±1.2	67.5∓1.2	<0.1	2.1
500	49.9±1.3	49.8∓1.3	<0.2	1.0	32.3±1.1	67.6∓1.1	<0.1	2.1
600	45.5±2.4	54.3∓2.4	<0.2	1.2	28.7±1.1	70.8∓1.1	<0.5	2.5
700	40.0±1.3	59.7∓1.3	<0.3	1.5	26.3±1.0	73.2∓1.0	<0.5	2.8
800	35.1±1.3	64.6∓1.3	0.3±0.1	1.8	22.6±1.0	76.9∓1.0	<0.5	3.4
1000	27.2±1.0	72.4∓1.0	0.4±0.1	2.7	17.3±0.7	82.4∓0.7	0.3±0.1	4.8
1200	21.6±0.9	77.5∓0.9	0.9±0.1	3.6				
1500	15.9±0.7	83.2∓0.7	1.0±0.1	5.2	10.3±0.5	89.1∓0.5	0.6±0.1	8.6
2000	10.6±0.5	88.3∓0.5	1.1±0.1	8.4	8.1±0.4	91.0∓0.4	0.9±0.1	11.2
3000	6.5±0.3	90.6∓0.3	2.9±0.1		5.0±0.2	93.4∓0.2	1.6±0.1	

lation of the molecular constants of the deeply bound states is given in Table V.

From Table V, it can be seen that the calculated equilibrium separation for the $X\,^2\Sigma$ state of CaH is at an R value which is greater than the spectroscopic value by ~ 0.05 Å. This shift is expected, because CaH in the well region is dominated by the ion-pair state composed of Ca^+-H^-. As seen from the atomic calculations, the ion-pair state dissociates to a level that is 0.20 eV below the true value.[19] Hence, the Coulomb potential of the ion-pair shifts the R_e for the $X\,^2\Sigma$ state of CaH to an internuclear separation that is too large. The calculated dissociation energy, however, is in good agreement with the experiment.

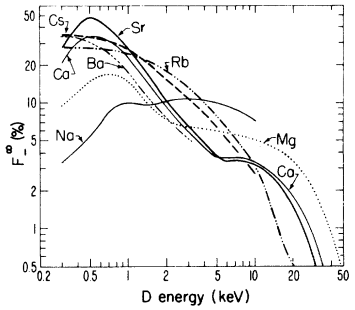

FIG. 9. Composite of F^{∞}_{-} fractions produced in metal vapors. Data from other laboratories are included.

As observed by Saxon *et al.*[20] in their calculations on MgH, a full valence CI including triple excitations only increases the dissociation energy by 0.0034 eV over the singles and doubles CI result. A similar behavior is expected for CaH, and it is concluded that the calculation for the dissociation energy is very close to the full valence electron CI limit.

The $X\,^1\Sigma$ state of CaH^- was found to be bound and stable to electron autodetachment. The calculated adiabatic molecular electron affinity for the $v'=0$ to $v''=0$ transition is 0.766 eV. If the negative-ion and neutral potentials are shifted to their true asymptotic separation, the adiabatic electron affinity increases to 0.905 eV. Hence, it is unequivocal that the CaH^- molecular ion is stable and

TABLE III. Interaction potential energies for the $X\,^2\Sigma$ and $X\,^1\Sigma$ molecular states of CaH and CaH^- determined by the V method of calculation. The units are 10^{-3} h (1 h=27.211 652 eV), and the values are given relative to the asymptotic energy separations of −677.286 73 h and −677.309 35 h for CaH and CaH^-, respectively.

R (a_0)	CaH-$X\,^2\Sigma$	CaH^--$X\,^1\Sigma$
2.5	66.91	74.40
2.75	11.01	16.83
3.0	−25.32	−21.32
3.25	−47.38	−45.40
3.5	−59.31	−59.55
3.75	−64.24	−66.88
3.8	−64.60	
3.85	−64.79	−68.43
3.9	−64.82	−68.97
3.95	−64.70	−69.37
4.0	−64.45	−69.63
4.05		−69.78
4.1		−69.82
4.15		−69.77
4.25	−61.55	−69.39
4.5	−56.68	−67.25
5.0	−44.04	−60.09
5.5	−30.48	−51.69
6.0	−18.04	−43.59
7.0	− 4.56	−30.11
8.0	− 0.99	−20.49
10.0	− 0.13	− 9.54
15.0	− 0.01	− 1.88
20.0	− 0.00	− 0.57
25.0	− 0.00	− 0.23
30.0	− 0.00	− 0.11

deeply bound.

Besides the V calculation for the $X\,^1\Sigma$ state of CaH^+, a large CV calculation has been performed to determine accurately the potential parameters. The results of this calculation are given in Table VI, and the molecular constants are summarized in Table V. It has been estimated that the CV value for R_e is accurate to ±0.02 Å and that D_e is accurate to ±0.05 eV. For future comparison to spectroscopic data, the $\Delta G(v+\frac{1}{2})$ values for the CV potential are given in Table VII. The CV method was also used to calculate the second $^1\Sigma$ state of CaH^+ but, because it is less reliable, its molecular constants are simply listed here: $R_e=2.33$ Å, $D_e=1.10$ eV, $\omega_e=804$ cm^{-1}, $\omega_e X_e=1.56$ cm^{-1}, $B_e=31.6$ cm^{-1}, and $\alpha_e=0.055$ cm^{-1}. The spectroscopic constants were computed in the same manner as in Table V.

TABLE IV. Interaction potential energies for the $X\,^1\Sigma$ and $a\,^3\Sigma$ molecular states of CaH^+ determined by the V method of calculation. The units are 10^{-3} hartrees, and the values are given relative to the asymptotic energy separation of −677.069 153 h.

R (a_0)	$X\,^1\Sigma$	$a\,^3\Sigma$
2.5	35.368	170.422
2.75	16.711	120.400
3.0	−49.027	84.686
3.25	−67.205	59.521
3.5	−75.492	41.965
3.7	−77.138	31.882
3.75	−77.024	29.791
3.8	−76.734	27.849
4.0	−74.087	21.359
4.25	−68.339	15.490
4.5	−60.976	11.358
4.75	−52.871	8.396
5.0	−44.666	6.225
5.5	−29.707	3.354
6.0	−18.297	1.644
8.0	− 2.156	−0.362
9.0	− 0.845	−0.363
10.0	− 0.397	−0.275
15.0	− 0.054	−0.054
20.0	− 0.017	−0.017
25.0	− 0.007	−0.007
30.0	− 0.003	−0.003

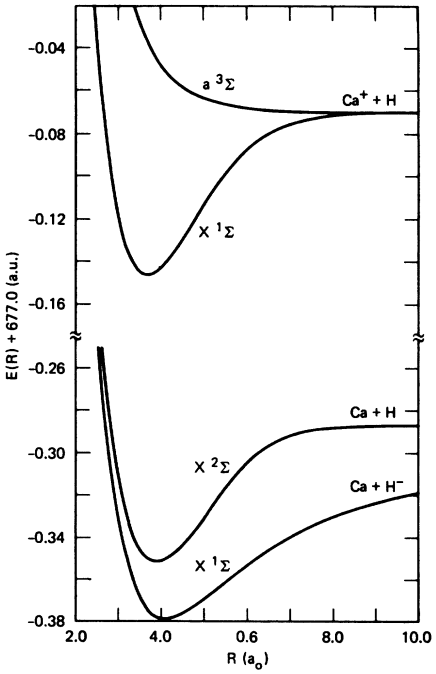

FIG. 10. *Ab initio* potential energy calculations for the molecular states dissociating to the ground states of CaH^+, CaH, and CaH^-. The values are from the (V) CI calculations.

TABLE V. Molecular constants (spectroscopic constants calculated by using the four lowest vibrational levels; experimental data from Ref. 18).

Molecule	State	Method	R_e (Å)	D_e (eV)	D_0 (eV)	ω_e (cm^{-1})	$\omega_e X_e$ (cm^{-1})	B_e (cm^{-1})	α_e (cm^{-1})
CaH^+	$X\,^1\Sigma$	CV	1.881	2.166	2.073	1504.5	21.01	4.85	0.0985
		V	1.955	2.099	2.010	1445.1	19.97	4.48	0.0908
CaH	$X\,^2\Sigma$	V	2.055	1.764	1.686	1268.7	18.52	4.06	0.0922
		Expt.	2.003		≤ 1.70	1298.3	19.10	4.28	0.0970
CaH^-	$X\,^1\Sigma$	V	2.167	1.900	1.837	1035.1	21.78	3.65	0.1153

By using the spectroscopic value for the ionization potential[18] of calcium and the dissociation energies D_0 given in Table V, it was possible to estimate the molecular ionization potential for CaH as 5.72 eV. The experimental value[19] is 5.86 ± 0.09 eV. It is doubtful that the calculated value has a larger uncertainty than ± 0.10 eV. Therefore, because the transition is near vertical, it is concluded that the experimental value is at least 0.05 eV too great.

By referring to the neutral and negative-ion-potential curves given in Fig. 10, it can be concluded that the electron detachment cross section σ_{-0} for $H^- + Ca \rightarrow H + Ca + e^-$ will be exceedingly small in the molecular collision regime $E \leq 1$ keV. This prediction is based on the observation that the negative-ion and neutral states are well separated at all calculated internuclear distances. Coupling of the negative-ion state to the continuum will be small, because there is no direct crossing into the continuum as observed for H^- + rare-gas systems[21] nor is the electron loss mediated by a charge-transfer state as in the H^- + alkali systems.[22] It is predicted that the electron-detachment cross section will decrease rapidly with decreasing energy below 1 keV. At higher energies, this cross section will be due simply to the impact ionization of the H^- and will increase in the low-keV regime.

Correspondingly, because the negative-ion equilibrium yield is equal to the negative-ion-formation cross section divided by the sum of it and the detachment cross section, [Eq. (5)], systems possessing a small detachment cross section relative to the formation cross section will have high yields. Such

TABLE VI. Interaction potential energies for the $X\,^1\Sigma$ molecular state of CaH^+ determined by the CV method of calculation. The units are 10^{-3} hartrees, and the values are given relative to the asymptotic energy separation of $-677.090\,935$ h.

R (a_0)	$X\,^1\Sigma$
2.5	8.457
2.75	−35.724
3.0	−61.724
3.25	−74.976
3.4	−78.518
3.5	−79.475
3.55	−79.597
3.6	−79.506
3.7	−78.761
4.0	−73.078
4.25	−65.818
4.5	−57.458
4.75	−48.797
5.0	−40.414
5.5	−25.960
6.0	−15.627
8.0	− 1.847
10.0	− 0.367
20.0	− 0.016
25.0	− 0.007
30.0	− 0.003

TABLE VII. $\Delta G(v+\frac{1}{2})$ values for the $X\,^1\Sigma$ state of CaH^+ calculated via the CV method.

v	$\Delta G(v+\frac{1}{2})$ (cm^{-1})
0	1461.8
1	1417.8
2	1372.6
3	1325.8
4	1277.2
5	1226.1
6	1172.0
7	1114.3
8	1051.9
9	983.7
10	908.3
11	827.2
12	743.2
13	646.9

behavior appears to be prevalent for the heavier alkaline-earth target systems.

VI. CONCLUSIONS

Equilibrium charge-state fractions in the energy range 0.3 to 3 keV have been measured for deuterium ions and atoms in magnesium, calcium, strontium, and barium vapors. F_-^∞ values show excellent agreement with earlier measurements above 1.2 keV. No measurements exist for comparison below 1.2 keV. The large F_-^∞ values at lower energies are in general accordance with the theoretical calculations. These indicate that the electron-detachment cross section σ_{-0} will be small at $E \leq 1$ keV. The D^- yield of 50% in strontium vapor at 500 eV is appreciably larger than for any other target material observed to date. Line densities of the order of 2×10^{15} cm^{-2} are sufficient to approach equilibrium and are achievable with either jets or vapor targets of reasonable length and temperature.

Ab initio CI interaction energies are presented for the molecular states arising from the ground states of CaH^+, CaH, and CaH^-. The ground molecular states are found to be deeply bound, $D_e > 1.7$ eV, and the negative-ion state is predicted to be stable to electron autodetachment. Electron detachment in collisions of D^- with calcium and with heavy alkaline-earth atoms is concluded to proceed with small cross sections at energies less than 1 keV. Such behavior is consistent with the negative-ion equilibrium measurements presented in this paper.

ACKNOWLEDGMENTS

We very much appreciate the assistance provided by the technical groups at LBL and by Dr. R. V. Pyle and Dr. W. Kunkel. The work was supported by the Office of Fusion Energy and the U. S. Department of Energy under Contract No. W-7405-ENG-48 and DEAT03-76ET53025 and the University of Missouri—Rolla. The joint studies agreement with IBM—San Jose was beneficial.

*Permanent address: University of Missouri-Rolla, Rolla, Missouri 65401.

†Permanent address: IBM Research Laboratory, Monterey and Cottle Roads, San Jose, California 95193.

[1]A. S. Schlachter, K. R. Stalder, and J. W. Stearns, Phys. Rev. A 22, 2494 (1980).

[2]K. H. Berkner, D. Leung, R. V. Pyle, A. S. Schlachter, and J. W. Stearns, Nucl. Instrum. Methods 143, 157 (1977).

[3]K. H. Berkner, D. Leung, R. V. Pyle, A. S. Schlachter, and J. W. Stearns, Phys. Lett. 64A, 217 (1977).

[4]T. J. Morgan, J. Stone, M. Mayo, and J. Kurose, Phys. Rev. A 20, 54 (1979).

[5]R. E. Olson, Report No. BNL-51304, 1980, p. 106 (unpublished).

[6]R. H. McFarland and A. H. Futch, Jr., Phys. Rev. A 2, 1795 (1970).

[7]K. H. Berkner, T. J. Morgan, R. V. Pyle, and J. W. Stearns, Phys. Rev. A 8, 2870 (1973).

[8]R. R. Hultgren, P. D. Desai, D. T. Hawkins, M. Gleiser, K. K. Kelley, and D. D. Wagman, *Selected Values of the Thermodynamics Properties of the Elements* (American Society of Metals, Metals Park, Ohio, 1973).

[9]K. H. Berkner, B. R. Meyers, and R. V. Pyle, Rev. Sci. Instrum. 39, 1204 (1968).

[10]M. W. Geis, K. A. Smith, and R. D. Rundel, J. Phys. E 8, 1011 (1975).

[11]B. Liu, K. O. Ohata, and K. Kirby-Docken, J. Chem. Phys. 67, 1850 (1977).

[12]A. W. Weiss, Phys. Rev. 122, 1826 (1961).

[13]H. Hotop and W. C. Lineberger, J. Phys. Chem. 4, 539 (1975) (reference data).

[14]E. Clementi and C. Roetti, At. Data Nucl. Data Tables 14, 177 (1974).

[15]B. Liu and R. E. Olson, Phys. Rev. A 18, 2498 (1978).

[16]C. E. Moore, *Atomic Energy Levels*, Natl. Bur. Stand. (U.S.) Circ. No. 467 (U.S. GPO, Washington, D.C., 1949), Vol. 1.

[17]T. M. Miller and B. Bederson, Phys. Rev. A 14, 1576 (1976).

[18]E. A. Reinsch and W. Meyer, Phys. Rev. A 14, 915 (1976).

[19]K. P. Huber and G. Herzberg, *Constants of Diatomic Molecules* (Van Nostrand Reinhold, New York, 1979).

[20]R. P. Saxon, K. Kirby, and B. Liu, J. Chem. Phys. 69, 5301 (1978).

[21]R. E. Olson and B. Liu, Phys. Rev. A 17, 1568 (1978).

[22]R. E. Olson and B. Liu, J. Chem. Phys. 73, 2817 (1980).